CLM - P 376

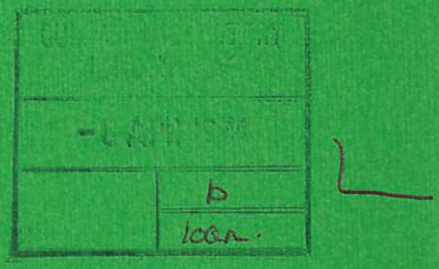

UKAEA RESEARCH GROUP

Preprint

AN EXPERIMENTAL INVESTIGATION OF SLOW MODE SHOCK WAVES

A D CRAIG

CULHAM LABORATORY
Abingdon Berkshire

1973

CLM - P 376

AN EXPERIMENTAL INVESTIGATION OF SLOW MODE SHOCK WAVES

by

A.D. CRAIG

(Submitted for publication in Journal of Plasma Physics)

ABSTRACT

An idealised, one-dimensional theoretical model is presented of a novel method of launching a slow mode hydromagnetic shock wave. The reduction of the transverse magnetic field component at the boundary of a semi-infinite plasma containing a uniform oblique magnetic field results in the propagation of a fast mode expansion wave followed by a slow mode shock.

An experiment designed to test this launching method is described. An initial hydrogen plasma containing axial and azimuthal magnetic field components is set up in a large annular apparatus. The azimuthal field is then reversed at one end of the device by a fast rising radial discharge. Diagnosis of the resulting flow with small magnetic and electric probes shows the propagation of the fast expansion wave and slow shock but also a third wave, having the properties of a 'piston', follows. When the theory is extended to include a moving boundary, i.e. the 'piston', good quantitative agreement is obtained with the experimental results.

The annular geometry of the experiment leads to centrifugal effects not considered in the one dimensional theory but these are not sufficient to disrupt seriously the main flow pattern.

Detailed measurements of the shock indicate a dispersive structure.

UKAEA Research Group,
Culham Laboratory
Abingdon,
Berkshire

December, 1973

CONTENTS

1. INTRODUCTION

In this paper we expand on an earlier letter (Craig and Paul, 1973) which describes what we believe to be the first detailed laboratory investigation of slow mode hydromagnetic shock waves.

There have been many reports of laboratory experiments which produce fast mode shock waves propagating into plasmas containing magnetic fields of various magnitudes and directions (Paul et al, 1965; Robson and Sheffield, 1969; Craig and Paul, 1973). Such shocks are associated with the steepening of fast mode MHD waves. Slow mode MHD waves can also, in principle, steepen into shock waves (Bazer and Ericson, 1958) but such shocks are not so easily launched.

Space satellite measurements of velocity, number density, ion temperature and magnetic field have demonstrated the presence of discontinuities in the solar wind satisfying the conservation relations for a slow shock wave (Chao and Olbert, 1970; Burlaga and Chao, 1971) but it is not clear why such shocks should form.

The existence of slow shocks is invoked in certain astrophysical theories. An example is in the model of a solar flare proposed by Petschek (1963) where the flow pattern of plasma and magnetic field involves the presence of two pairs of stationary slow shocks emanating from a magnetic neutral point. In an experimental study of magnetic flux transfer at such a x-type neutral point in a double inverse pinch device (Bratenahl and Yeates, 1970) the formation of such slow shock pairs has been observed.

Section 2 briefly outlines the main properties of slow shocks. In section 3 a full theory of the shock launching process is presented. Sections 4 and 5 give details of the apparatus and initial plasma respectively. In section 6 the experimental results are presented and comparison with theory made.

2. PROPERTIES OF SLOW MODE SHOCKS

In a magnetised plasma there are three anisotropic velocities for small amplitude waves, slow c_s, intermediate c_i and fast c_f. Fast waves involve changes in density ρ and transverse magnetic field B_T which are of the same sign, and, when compressive, they can steepen into fast shocks through which both ρ and B_T increase. Slow waves also involve changes in ρ and B_T but of opposite sign and again, when compressive, they can steepen into

slow mode shocks through which ρ increases but B_T decreases. Intermediate waves, on the other hand, simply rotate B_T and should not form a shock. Whereas fast waves can propagate in any direction in a magnetised plasma, slow and intermediate waves require a field component parallel to the direction of propagation.

For a shock to be stable to perturbations, the change of flow speed, $v_1 \rightarrow v_2$, across the shock (for a frame of reference moving with the shock) must cross only one linear wave speed (Anderson, 1963). Thus the velocity conditions of a general slow shock are

$$c_{f1} > c_{i1} > v_1 > c_{s1}$$
$$c_{f2} > c_{i2} > c_{s2} > v_2$$

where the suffices 1 and 2 refer to preshock and postshock conditions respectively. A special case where the stability condition is not straight-forward is the so-called 'switch-off' shock. This is the strongest possible slow shock for a given set of pre-shock plasma parameters and is characterised by

$$B_{T2} = 0$$
$$v_1 = c_{i1}$$

The stability condition therefore does not classify the 'switch-off' shock solution. The so-called 'switch-on' shock solution of fast parallel shocks has an analogous marginal stability but has been shown experimentally to

be stable (Craig and Paul, 1973).

The decrease in B_T in a slow shock requires an electric current. The interaction of this current with the normal magnetic field component in the shock produces a transverse flow velocity behind the shock. The magnetic energy decreases through the shock and is shared between increased thermal and transverse kinetic energy behind the shock. Further details of slow mode shock transitions are discussed in the review by Kantrowitz and Petschek (1966).

3. THEORY OF SHOCK LAUNCHING PROCESS

3.1 Ideal MHD Model

We discuss the principle of our laboratory slow shock formation using a one-dimensional plane Cartesian model although the experiment is in fact performed in an annular geometry. Cylindrical coordinate notation is used in order that theory may be more easily related to the experiment.

We consider a semi-infinite plasma (density ρ_o, temperature T_o) containing initial magnetic field components $B_{\theta o}$ and B_{zo} and bounded by a solid insulating interface 'A' at $z = 0$ (Fig.1(a)). This plasma is perturbed by an instantaneous decrease in B_θ at the interface produced by a radial current ($- J_r$). A qualitative and then quantitative description of the flow is given below.

If $B_{\theta o}$ is reduced at the interface by an infinitesimal amount δB_θ it is clear that the initial conditions of the plasma must be matched to the new boundary condition through one or more linear waves. One possibility exists. A fast wave will propagate at a velocity c_f transmitting a decrease in B_θ and ρ but in order to conserve mass a further wave must propagate; this can only be a slow wave with velocity c_s in which B_θ decreases further to the interface value and ρ increases. A current $(-J_r)$ flows in both waves. The axial force $(-J_r B_\theta)$ in the fast wave produces axial plasma motion $(-V_z)$ back towards the interface whilst the force $J_r B_z$ produces a transverse plasma motion in the θ direction. A further increase in V_θ is produced by the force $J_r B_z$ in the slow wave. The increase in density and temperature across the slow wave must balance the axial magnetic force $(-J_r B_\theta)$ and stop the plasma in order to satisfy the condition $V_z = 0$ at the interface.

In approaching the non-linear flow problem we use the method of characteristics in which large amplitude waves are reduced to a series of successive small amplitude step-function waves propagating at linear wave velocities into the plasma conditions left by previous waves. Successive fast waves will propagate more slowly in the laboratory frame of reference because c_f is reduced by the preceeding

waves and the propagation is into plasma moving in the opposite direction. However, successive slow waves will propagate more quickly in the laboratory frame of reference because c_s is increased by the preceding waves and therefore will steepen to form a slow shock wave. The nature of the general flow pattern is therefore as illustrated in Fig.1(b); a fast expansion wave is followed by a slow shock. We denote the regions 0, 1 and 2 as shown.

In order to calculate the quantitative details of the flow pattern we make the following assumptions:

(i) The plasma is non-dissipative, i.e. electrical conductivity $\sigma = \infty$ and viscosity $\nu = 0$.

(ii) The field perturbation at the interface is a step function. The problem then has conical similarity, i.e. flow properties are constant along straight lines eminating from the origin in the zt plane and can change only across such lines.

(iii) The gas pressure is isotropic and obeys the perfect gas law, i.e. $p = A\rho^{\gamma} = 2\, n_e\, kT$.

We use the ideal MHD equations for a non-dissipative medium, i.e.

$$\frac{\partial \rho}{\partial t} + \nabla \cdot (\rho \underline{v}) = 0 \qquad \ldots (1)$$

$$\rho \frac{\partial \underline{v}}{\partial t} + \rho \underline{v} \cdot \nabla \underline{v} + \nabla p - \frac{(\nabla \times \underline{B}) \times \underline{B}}{\mu} = 0 \qquad \ldots (2)$$

$$\frac{\partial \underline{B}}{\partial t} - \nabla \times (\underline{v} \times \underline{B}) = 0 \qquad \ldots (3)$$

$$\frac{\partial}{\partial t}\left(\frac{p}{\rho^{\gamma}}\right) + \underline{v} \cdot \nabla \left(\frac{p}{\rho^{\gamma}}\right) = 0 \qquad \ldots (4)$$

$$\nabla \cdot \underline{B} = 0 \qquad \ldots (5)$$

The above equations may be integrated across a small amplitude step function wave to give the following relations for the first order changes across such a wave.

$$- c\delta\rho + \rho\delta v_z = 0 \qquad \ldots (6)$$

$$- \rho c\delta v_z + \delta p + \frac{B_\theta \delta B_\theta}{\mu} = 0 \qquad \ldots (7)$$

$$\rho c\delta v_\theta + \frac{B_z \delta B_\theta}{\mu} = 0 \qquad \ldots (8)$$

$$B_\theta \delta v_z - c\delta B_\theta - B_z \delta v_\theta = 0 \qquad \ldots (9)$$

$$c\left(\delta p - \frac{\gamma p}{\rho}\delta\rho\right) = 0 \qquad \ldots (10)$$

$$\delta B_z = 0 \qquad \ldots (11)$$

where c is the propagation velocity. It is assumed that $\underline{B}$ and $\underline{v}$ remain in the θz plane, i.e. intermediate waves are not considered.

Equations (6) to (11) yield the following expression for c:

$$c^4 - c^2(a^2 + b_\theta^2 + b_z^2) + a^2 b_z^2 = 0 \qquad \ldots (12)$$

where

$$a^2 = \frac{\gamma p}{\rho} \quad , \quad b_\theta^2 = \frac{B_\theta^2}{\mu\rho} \quad , \quad b_z^2 = \frac{B_z^2}{\mu\rho} \; .$$

The two roots of equation (12) are c_f and c_s.

From equations (6), (7), (8) and (10) we obtain (Kantrowitz and Petschek, 1966)

$$\left(\frac{dB_\theta}{d\rho}\right)^2 - \left[1 + \left(\frac{B_\theta}{B_z}\right)^2 - \left(\frac{\rho}{\rho_o}\right)^\gamma\right]\left(\frac{B_z^2}{\rho B_\theta}\right)\frac{dB_\theta}{d\rho} - \left(\frac{B_z}{\rho_o}\right)^2\left(\frac{\rho}{\rho_o}\right)^{\gamma-2} = 0 \qquad \ldots (13)$$

where

$$\rho_o = \left(\frac{\mu\gamma A}{B_z^2}\right)^{-1/\gamma}$$

Equation (13) may be factored to give two first order differential equations describing the changes in the $B_\theta\rho$ plane for fast and slow waves. For fast waves $\frac{dB_\theta}{d\rho}$ is positive and for slow waves $\frac{dB_\theta}{d\rho}$ is negative.

Integration through the fast expansion wave (Fig.1(b)) was achieved by treating it as a series of small amplitude step function waves each with a fixed incremental change in ρ. The corresponding increments in B_θ, v_z and v_θ were calculated using equations (13), (6) and (8) respectively. After each step c_f was recalculated and the velocity of the next small amplitude wave in the laboratory frame, calculated as $C_z = c_f - V_z$.

The conservation relations across the slow shock are

$$\rho_2 v_{z2} = \rho_1 v_{z1} \qquad \ldots (14)$$

$$\rho_2 v_{z2}^2 + p_2 + \frac{B_{\theta 2}^2}{2\mu} = \rho_1 v_{z1}^2 + p_1 + \frac{B_{\theta 1}^2}{2\mu} \qquad \ldots (15)$$

$$\rho_2 v_{z2} v_{\theta 2} - \frac{B_z B_{\theta 2}}{\mu} = -\frac{B_z B_{\theta 1}}{\mu} \qquad \ldots (16)$$

$$\rho_2 v_{z2}\left(\frac{\gamma}{\gamma-1}\frac{p_2}{\rho_2} + \frac{v_{z2}^2}{2} + \frac{v_{\theta 2}^2}{2}\right) + \frac{B_{\theta 2}}{\mu}\left(B_{\theta 2} v_{z2} - B_z v_{\theta 2}\right)$$

$$= \rho_1 v_{z1}\left(\frac{\gamma}{\gamma-1}\frac{p_1}{\rho_1} + \frac{v_{z1}^2}{2}\right) + \frac{B_{\theta 1}^2 v_{z1}}{\mu} \qquad \ldots (17)$$

$$v_{z2} B_{\theta 2} - v_{\theta 2} B_z = v_{z1} B_{\theta 1} \qquad \ldots (18)$$

where the frame of reference is moving in the z direction with the shock and in the θ direction such that $v_{\theta 1} = 0$.

As boundary conditions we specify $B_{\theta 2}$ which is determined by the total applied radial current and in order to conserve mass at the interface ($z = 0$) we have

$$v_{z2} = V_s \quad \text{(the slow shock velocity)} . \qquad \ldots (19)$$

For any particular set of parameters in region (1) there is only one slow shock solution satisfying equations (14) to (19); this solution defines $B_{\theta 2}$. More specifically for a given $B_{\theta 2}$ the parameters in region (1) are determined. In deriving the full flow pattern we have halted the integration through the expansion wave at the point giving the required value of $B_{\theta 2}$.

An example using typical experimental initial parameters ($B_{zo} = 0.1\ T$, $B_{\theta o} = 0.2\ T$, $T_{eo} = 10^4\ K$, $n_{eo} = 7 \times 10^{20} m^{-3}$) is shown in Fig.2(a). The slow shock is of the 'switch-off' type, i.e. $B_{\theta 2} = 0$. Profiles of the various parameters are shown for $t = 1\ \mu s$.

It is also interesting to consider the flow pattern for the case where the perturbation field exceeds $B_{\theta o}$. The field reversal required in the flow pattern can only occur within a large amplitude intermediate wave. Such a wave would propagate at some point between the slow shock and the back of the expansion wave.

The properties of large amplitude intermediate waves are:

(i) They rotate the transverse field component through an arbitrary large angle (180^{o} in this case) whilst maintaining its amplitude constant.

(ii) The transverse velocity changes across the wave according to $\Delta \underline{v} = \Delta \underline{B} / (\mu\rho)^{\frac{1}{2}}$ where $\Delta \underline{B}$ is the change in transverse field.

(iii) No changes occur in the normal velocity component or the thermodynamic properties.

Thus for initial parameters as in Fig.2(a) but with $B_{\theta 2} = -\ 0.1\ T$ the flow pattern is as illustrated in Fig.2(b). As $B_{\theta 2}$ approaches zero the shock velocity increases whilst the intermediate wave velocity decreases until at $B_{\theta 2} = 0$ the two structures merge into the switch-off shock of Fig.2(a).

3.2 Non Ideal Effects

The experimental results described later have led us to extend the above model to include a non-ideal MHD effect. Because viscosity is assumed to be zero the above model shows the transverse velocity component V_θ behind the shock to persist right up to the end insulator. It is this motion which cancels the applied electric field $\underline{E}_r$,

$$\underline{E}_r + \underline{V}_\theta \times \underline{B}_z = 0$$

and prevents J_r currents flowing in the bulk of the plasma.

In practice the end insulator must impose boundary conditions, not only $V_z = 0$, but also $V_\theta = 0$. In a real plasma there must, therefore, be a viscous layer to match the transverse velocity of the plasma to the stationary boundary. Because E_r is then no longer cancelled, radial current will flow in this layer. The force on this current, $\underline{J}_r \times \underline{B}_\theta$, is directed towards the end insulator for $B_\theta \geq 0$ and so the viscous layer does not propagate. The change in B_θ across the layer weakens both the shock and expansion wave.

If, on the other hand, B_θ substantially reverses at the boundary, then the force $\underline{J}_r \times \underline{B}_\theta$ drives the viscous layer away from the insulator thus forming a piston. The insulator is now in a vacuum and the plasma boundary

conditions are effectively transferred to the piston which has both V_z and V_θ components of velocity.

Having introduced this new piston phenomenon from non-ideal MHD, we can return to our ideal MHD model but include the piston as a discontinuity with specified axial velocity (V_p). Thus

$$v_{z2} = V_s - V_p \qquad \ldots (20)$$

replaces equation (19) as the boundary condition. Again $B_{\theta 2}$ behind the shock is specified. Using the same method as in Section 3.1 we have computed a flow pattern for conditions relevant to the experiment (Fig.2(c)).

4. THE APPARATUS

The apparatus is shown schematically in Fig.3. The vacuum vessel consists of a pyrex glass cylinder (1.25 m long, 0.46 m diameter) with stainless steel end plates. Hydrogen was used in all the experiments discussed in this paper with filling pressures typically 20 mtorr.

A slow rising (10 msec) axial magnetic field (B_{zo}) of up to 0.28 Tesla is produced by a capacitor bank and a set of six coils. The coil current is clamped at its peak and the field remains essentially constant throughout the period of the discharge. The field is uniform to within 2% throughout the main volume of the discharge chamber.

An initial plasma is produced by an oscillatory axial current (100 μs period, 110 kA peak) between the annular electrode at the launch end and the far end plate. The current damps over five half cycles and is zero for $t > 250\ \mu s$.

An azimuthal field ($B_{\theta o}$) is produced at the end of the preheating discharge by passing an oscillatory current (200 μs period, currents up to 150 kA) through a central conductor. At peak values $B_{\theta o}$ remains essentially constant for the duration of the main launching discharge.

The main radial discharge is produced by applying an electric field $E_o \sim 200$ kV/m between a long central cylinder electrode ($\ell = 0.9$ m, dia. = 80 mm) surrounding the $B_{\theta o}$ conductor and the outer annular electrode used for the preheating discharge. The capacitor bank is in halves feeding opposite sides of the apparatus through transmission lines. A two stage pulse shaping circuit gives a first approximation to a square wave with the current rising in 0.5 μs to a peak $I_p = 180$ kA and remaining approximately constant for 3 μs.

This apparatus, without the $B_{\theta o}$ facility, has been used previously for fast shock studies (Craig and Paul, 1973).

5. INITIAL PLASMA

On initiating the $B_{\theta o}$ bias field current a current loop was induced in the initial plasma; this decayed in $\sim 10\,\mu s$ such that the vacuum r^{-1} distribution existed in $B_{\theta o}$ at the times of its peaks.

The radial and axial distribution of electron density $n_e(r,z,t)$ and temperature $T_e(r,z,t)$ have been measured using double Langmuir probes which had previously been calibrated by a helium-neon laser interferometer, (Craig and Paul, 1973).

The radial density distribution shows the presence of 50 mm thick low density sheaths adjacent to the centre electrode and the outer wall. However a region of reasonably uniform density existed for $80 < r < 180$ mm.

Fig.4 shows the axial distribution of density at times corresponding to the first ($t = 300\,\mu s$ after initiating preheating discharge) and second ($t = 400\,\mu s$) peaks of the $B_{\theta o}$ bias field. Due to the improved axial density distribution we have chosen to delay initiating the main launch discharge until the second peak of the $B_{\theta o}$ bias field. The Langmuir probe indicated an electron temperature of $\sim 1.5 \times 10^4$ K at this time.

6. EXPERIMENTAL OBSERVATIONS

6.1 General Flow Pattern

The experimental flow pattern has been deduced from measurements of the magnetic field using small magnetic probes (coils (dia. = 1.2 mm) encapsulated in epoxy resin spheres (dia. = 2.5 mm) and supported on 1.2 mm dia. ceramic rods; good frequency response to 10 MHz).

When B_θ is reduced or cancelled at the insulator the current remains near the insulator and nothing is observed to propagate. This can be explained by assuming that the radial current in the viscous layer so weakens the expansion wave that it is not seen and so weakens the slow shock that it does not separate.

When the applied current is sufficient to substantially reverse B_θ at the interface, a structure typified by the oscillogram of Fig.5 is seen by a B_θ magnetic probe position at $z = 140$ mm, $r = 142.5$ mm. The general structure is as predicted in Fig.2(c). The broad region of decreasing B_θ we identify as the fast expansion wave. This is followed by a short plateau region and then a sharp decrease in B_θ to almost zero. This latter we identify as a slow, almost switch-off, shock. Behind the shock is another plateau before B_θ increases in the opposite direction in what we identify as the piston.

The slight increase in B_θ following the main decrease of the shock is a reproducible feature and is discussed in Section 6.7.

6.2 Axial Propagation

A series of oscillograms such as Fig.5, but at $r = 125$ mm, have been analysed to produce the $B_\theta(z)$ distributions of Fig.6. The propagation of the expansion wave, shock and piston can be clearly seen. The magnitude of the applied radial current is such as to approximately reverse B_θ at the insulator. For the 2 μs distribution it is seen that between the piston and the back insulator B_θ is constant, i.e. no radial current flows. This suggests that a near vacuum exists in this region and we are therefore justified in calling the slower current front a piston.

The detailed axial propagation of the various features is shown in Fig.7. Shock and piston are identified as the peak $\dot{B}_\theta$ points. The small standard deviation error bars show the reproducibility to be good. The trajectory of the leading edge of the expansion wave is tentatively shown but clearly there is some difficulty in positively identifying this feature. Although some acceleration occurs during the propagation, the front of the expansion wave, shock and piston are seen to separate with time. Typical velocity values ($z = 0.14$ m) are $V_{EW} = 1.8 \times 10^5$ m/sec,

$V_s = 1.2 \times 10^5$ m/sec and $V_p = 8 \times 10^4$ m/sec.

Fig.8 shows the axial variation of the changes in B_θ occuring within the fast expansion wave ($\delta B_{\theta EW}$) and the slow shock ($\delta B_{\theta s}$). It is seen that initially the shock is almost of the 'switch-off' type but the strength decreases continuously during the propagation. The decrease in $\delta B_{\theta T} (= \delta B_{\theta s} + \delta B_{\theta EW})$ with z is less at higher radii for reasons explained in the next section. The field change through the shock $\delta B_{\theta s}$ compared to the total change $\delta B_{\theta T}$ increases as the strength decreases.

6.3 Radial Variations

In Fig.9 the radial variation in arrival time of the various features are illustrated. The expansion wave arrives slightly earlier at lower radius due to higher c_{fo} in the higher $B_{\theta o}$ region. The shock is substantially plane in the region $110 < r < 165$ mm. Some tilting at higher radii occurs in the piston profile.

The changes in B_θ occurring within the shock ($\delta B_{\theta s}$) and expansion wave ($\delta B_{\theta EW}$) in this radial region are shown in Fig.10. The initial field level (r^{-1} dependence) is also shown. For $r > 130$ mm the field changes are large and the 'switch-off' condition is approached. For $r < 130$ mm the field change becomes smaller and for $r < 100$ mm the shock cannot be identified. The deviation of the total B_θ

change, $\delta B_{\theta T}$, from an r^{-1} distribution in the region $r < 130$ mm implies an axial plasma current flowing into the back of the shock wave. The radial density distribution of this current, calculated directly from $\delta B_{\theta T}(r)$, is also shown in Fig.10. Virtually none of the axial current feeding the shock and expansion wave actually flows in the copper electrodes in the region ahead of the piston. For $r \geqslant 130$ mm the radial current in the waves is conserved although the different ratio of $\delta B_{\theta s}$ and $\delta B_{\theta EW}$ implies a radial variation in the distribution of this current between shock and expansion wave. For $r \geqslant 180$ mm return axial current flows from the shock and expansion wave.

The axial current in the region $r < 130$ mm is subject to a $\underline{J}_z \times \underline{B}_\theta$ force in the outward radial direction. The main electrode was made of highly conducting copper in an effort to encourage axial current flow in the electrode such that no movement would result from this force. Behind the piston this was successful with $> 90\%$ of the axial current flowing in the electrode. The $\underline{J}_z \times \underline{B}_\theta$ force on any axial plasma current was therefore radially inward. Analysis of a series of $\delta B_{\theta T}$ versus r plots, such as Fig.10, show the region of axial current between the piston and shock to move out radially with a velocity of $\sim 7 \times 10^4$ m/sec. This movement is therefore not sufficiently fast to effect the shock in the region $r \geqslant 150$ mm during

the time of interest. The weakening of the shock and expansion wave during the axial propagation ($r = 125$ mm) shown in Fig.8 is largely due to this radial movement of the region of axial current.

6.4 Effect of Varying Axial Bias Field

Fig.11(a) shows the B_θ field changes through the shock and the expansion wave plotted as a function of B_{zo} for $r = 142.5$ mm, $B_{\theta o} = 0.13$ T. At higher B_{zo} a larger proportion of the total field change occurs in the expansion wave. For B_{zo} values outside the range of Fig.11(a) the shock became irreproducible. The arrival time of the shock, and hence probably the shock velocity, are virtually independent of B_{zo}.

6.5 Comparison with Theory

It is appropriate at this stage to compare the B_θ results of sections 6.1 to 6.4 with the theoretical results of section 3.2.

The boundary conditions and initial parameters, i.e. $n_{eo} = 5 \times 10^{20}$ m^{-3}, $T_o = 1.5 \times 10^4$ K, $B_{zo} = 0.15$ T, $B_{\theta o} = 0.13$ T, $V_p = 8 \times 10^4$ m/s, $B_{\theta 2} = 0.02$ T, of the theoretical flow pattern of Fig.2(c) were chosen to match the experimental conditions of sections 6.1 to 6.3 at $z = 140$ mm, $r = 142.5$ mm.

We are able to make direct comparisons between theory and experiment for the following parameters :

(i) the velocity of the front of the expansion wave (c_{fo});

(ii) the velocity of the shock (V_s);

(iii) the change in transverse field across the expansion wave ($\delta B_{\theta EW}$);

(iv) the change in transverse field across the shock ($\delta B_{\theta s}$).

Good agreement is obtained as shown in Table I.

TABLE I

	Experiment	Theory
c_{fo} (km/sec)	180	194
V_s (km/sec)	120	121
$\delta B_{\theta EW}$	- 0.03	- 0.033
$\delta B_{\theta s}$	- 0.08	- 0.077

The condition in front of the shock wave, obtained through the measured expansion $\delta B_{\theta EW}$, are plasma velocity $V_{z1} = -\ 2.0 \times 10^4$ m/sec (towards shock), $c_{s1} = 1.65 \times 10^4$ m/sec, $c_{i1} = 1.54 \times 10^5$ m/sec and $c_{f1} \approx c_{fo}$. Hence the velocity of the shock relative to the plasma $u_1 = V_s - V_{z1} = 1.4 \times 10^5$ m/sec and the corresponding Mach number $M_s = u_1/c_{s1} = 8.5$. The shock clearly satisfies the condition $c_{s1} < u_1 < c_{i1} < c_{f1}$ for a slow shock. It should be noted that the theory is for a steady state whilst experimentally Figs.7 and 8 show the boundary conditions V_p and $B_{\theta 2}$ to change slowly with z.

Fig.12(a) shows the theoretical variations of $\delta B_{\theta s}$, $\delta B_{\theta EW}$ and V_s on V_p for a fixed $\delta B_{\theta T}$. The ratio

$\delta B_{\theta s}/\delta B_{\theta T}$ is seen to increase with increased V_p. Fig.12(b) shows the variation of $\delta B_{\theta s}/\delta B_{\theta T}$ versus $\delta B_{\theta T}$ for a fixed V_p. No attempt is made here at a quantitative comparison between theory and the results of Fig.8, but the fact that experimentally the ratio $\delta B_{\theta s}/\delta B_{\theta T}$ increases with z, i.e. with higher V_p and lower $\delta B_{\theta T}$, is consistent with theory.

Fig.12(c) shows the theoretical variation of $\delta B_{\theta s}$, $\delta B_{\theta EW}$ and V_s on $B_{\theta o}$ for a fixed $\delta B_{\theta T}$ and V_p. The increased $\delta B_{\theta s}/\delta B_{\theta T}$ with $B_{\theta o}$, i.e. lower radii, is consistent with the experimental result of Fig.10 in the region $r > 130$ mm where axial currents are negligible.

Fig.12(d) shows the theoretical variation of $\delta B_{\theta s}$, $\delta B_{\theta EW}$ and V_s with B_{zo} for a fixed $\delta B_{\theta T}$ and V_p. Again the theoretical variation of $\delta B_{\theta s}/\delta B_{\theta T}$ is consistent with the experimental result of Fig.11. Further V_s is almost independent of B_{zo} as is found experimentally.

6.6 Relationship of Other Field Components

Fig.13 shows typical oscillograms of δB_z and δB_θ, and δB_z and B_r obtained from adjacent magnetic probes. Although the changes occurring in B_z and B_r are not predicted by the idealised one-dimensional theory of section 3, they can be understood in the context of the annular geometry of the experiment where the transverse

motion behind the expansion wave and shock constitutes a rotation which in the absence of an adequate centripetal force leads to outward radial motion of both plasma and associated axial field lines. The negative B_r signal between the shock and piston demonstrates the presence of such a motion. An azimuthal current

$$J_\theta = \frac{1}{\mu}\left(\frac{\partial B_r}{\partial z} - \frac{\partial B_z}{\partial r}\right)$$

is induced by the radial motion hence providing an inward radial force $\underline{J}_\theta \times \underline{B}_z$. The continuation of the negative B_r signal up to the piston however suggests this force is not sufficient to produce a radial momentum balance.

An axial force $\underline{J}_\theta \times \underline{B}_r$, directed away from the interface, also exists in the region between the shock and piston as a result of the radial motion. The peak magnitude of this force is approximately 0.5 times the peak $\underline{J}_r \times \underline{B}_\theta$ force within the shock. Thus, whilst the omission of this rotational term from the axial force equation of the idealised one dimensional theory is clearly important it is reasonable that it does not seriously disrupt the main flow pattern.

A small positive B_r peak, approximately coincident with the main B_θ decrease of the shock, precedes the negative B_r signal associated with the radial motion. It is suggested in the next section that this is part of the dispersive structure of the shock.

6.7 Shock Structure

For the purposes of previous discussion we have identified the steep decrease in B_θ as the slow shock wave. The radial variation in the temporal width of this structure, arbitrarily taken between the 20% peak $\dot{B}_\theta$ points, is shown in Fig.9. The field change occurs typically in $\sim 0.2\,\mu s$ which, with a velocity of 1.2×10^5 m/s, corresponds to a thickness of ~ 24 mm.

The oscillogram of Fig.5 however shows that, following the steep B_θ decrease of the shock, there is a slight increase in B_θ; this is seen on the $\dot{B}_\theta$ oscillogram as the small positive peak following the large negative peak of the main shock transition. This feature is reproducible and is shown below to be part of a dispersive shock structure. The other waves apparent in the $\dot{B}_\theta$ oscillogram in the region between the shock and piston are not reproducible and are probably not part of the shock structure.

We consider the two fluid theory of the low frequency dispersion curves in a magnetised plasma (Stringer, 1963). Dispersive effects appear on the slow magneto-acoustic branch for ω approaching $\omega_{ci} \cos\alpha$ where α is the angle between the direction of propagation and the initial magnetic field, and are such that higher frequency waves have a slower phase velocity. The phase velocity becomes

zero for $\omega = \omega_{ci} \cos\alpha$. Thus, as fast mode oblique shocks are characterised by forward dispersion of damped precursor whistler waves, so slow mode shocks are characterised by backward dispersion of damped magneto-acoustic waves. Theoretical structures of slow mode shocks demonstrating such dispersion have been computed by Bickerton et al, (1971). The wavelength of such magneto-acoustic waves is given by (Stringer, 1963)

$$\lambda = 2\pi M \left(\frac{s}{\omega_{ci}}\right)\left(\frac{M^2-1}{M^2 - \cos^2\alpha}\right)^{\frac{1}{2}}$$

where

$$s = \left[\frac{\gamma k (T_e + T_i)}{m_i}\right]^{\frac{1}{2}} = \text{sound speed}$$

$$M = \frac{v_p}{s}$$

where v_p = phase velocity of the wave.

We consider the slow shock of Fig.5. The measured distance between positive and negative $\dot{B}_\theta$ peaks, i.e. average $\lambda/2$, is ~ 20 mm. Inserting the following mid-shock conditions, $T_e + T_i = 3 \times 10^5$ K, $B_\theta = 0.06$ T, $|\underline{B}| = 0.16$ T, $\alpha = 22^\circ$, $v_p = 9 \times 10^4$ m/sec, (obtained from the measured structure and Fig.2(c)) into the above theoretical expression we again obtain $\lambda/2 \sim 20$ mm.

6.8 Electric Field Measurements

The electric field components can be derived from the generalised Ohms law, with electron inertia neglected, i.e.

$$\underline{E} + \underline{V} \times \underline{B} + \frac{1}{en_i}\left(\nabla p_e - \underline{J} \times \underline{B}\right) - \eta \underline{J} = 0.$$

Thus we have

$$E_r = \left[- V_\theta B_z + V_z B_\theta \right] + \frac{J_\theta B_z}{en_i} + \eta J_r$$

$$E_\theta = \left[- \frac{J_r B_z}{en_i} \right] - V_z B_r + V_r B_z$$

$$E_z = \left[\frac{J_r B_\theta}{en_i} - \frac{1}{en_i} \frac{\partial p_e}{\partial z} \right] - \frac{J_\theta B_r}{en_i} - V_r B_\theta + V_\theta B_r$$

In each of the above expressions the terms in square brackets are present in the idealised plane geometry model of section 3 whilst the remaining terms arise due to rotational effects.

Fig.14 shows typical oscillograms of the electric field components obtained from small, axially inserted electric probes each with the B_θ oscillogram obtained simultaneously from an adjacent magnetic probe. Knowing the magnetic field variation through the structure we may use the electric field variation to derive information concerning plasma velocity and electron pressure.

The current densities are obtained directly from the unintegrated $\dot{B}$ signals

$$J_r = \frac{1}{\mu V_s} \frac{\partial B_\theta}{\partial t}$$

$$J_\theta \sim \frac{1}{\mu V_s} \frac{\partial B_r}{\partial t}$$

Typically we find $J_{r_{max}} \sim 2 \times 10^6$ A/m^2 within the main shock transition and $J_{\theta_{max}} \sim 10^6$ A/m^2 in the region immediately behind the shock.

We consider the E_r component first. Using the theoretical values from Fig.2(c), behind the expansion wave

$- V_\theta B_z = 3.7 \times 10^3$ V/m ; $V_z B_\theta = 2.0 \times 10^3$ V/m ; $E_{r_{th}} \sim 5.7 \times 10^3$ V/m

and behind the shock

$- V_\theta B_z = 16.5 \times 10^3$ V/m ; $V_z B_\theta = -1.6 \times 10^3$ V/m ;

$\frac{J_{\theta_{max}} B_z}{en_i} = 1.0 \times 10^3$ V/m ; $E_{r_{th}} \sim 16 \times 10^3$ V/m .

If a classical resistivity is assumed the resistive term is negligible. These values of E_r are in reasonable agreement with the experimental values of Fig.14. Thus the theoretically predicted rotation behind the expansion wave and shock are directly demonstrated.

The E_θ and E_z components are dominated by rotational effects.

From the experimentally measured magnetic fields

$$\left(- \frac{J_r B_z}{en_i}\right)_{max} \sim 1.9 \times 10^3 \text{ V/m} ; \quad - V_z B_r \sim 10^4 \text{ V/m} .$$

Comparing this with the experimental E_θ of $\sim 1.4 \times 10^4$ V/m behind the shock suggests the presence of a V_r component of $\sim 3 \times 10^4$ m/s .

Within the main field transition of the shock we have

$$\left(\frac{J_r B_\theta}{en_i}\right)_{max} \sim - 1.3 \times 10^3 \text{ V/m}$$

This term is apparently dominant in the small negative E_z peak coincident with the main B_θ decrease of the shock. For the theoretical shock transition of Fig.2(c) and the measured shock thickness an estimate of the magnitude of the electron pressure term of E_z is

$$-\frac{1}{en_i}\frac{\partial p_e}{\partial z} \sim + \ 2.5 \times 10^3 \ \text{V/m}$$

and is therefore of opposite sign to the magnetic term discussed above. The steep positive experimental E_z signal occurring at the end of the main shock field transition is probably dominated by the heating-compression term but unfortunately cannot unambiguously be measured because of the rotational terms

$$V_\theta B_r \sim 10^4 \ \text{V/m} \ ; \quad \left(\frac{J_\theta B_r}{en_i}\right)_{max} \sim 6 \times 10^2 \ \text{V/m}$$

becoming dominant behind the shock.

7. SUMMARY

An idealised one-dimensional thecry is presented for a novel method of launching a slow mode shock wave. The assumption of ideal MHD leads to a flow pattern involving a transverse plasma flow adjacent to a stationary solid boundary. In a real experimental situation a viscous boundary layer must form within which a current flows; this serves to weaken the expansion wave and slow shock. For a large field perturbation at the boundary, such that B_θ is substantially reversed, the magnetic force on the viscous boundary layer is such as to propel it away from the boundary in a way characteristic of a piston. In addition to its axial motion this piston also has transverse motion arising from the $\underline{J}_r \times B_z$ force and thus can

match to the transverse flow behind the slow shock. The theory is extended to include a moving boundary.

The experiment is performed in annular geometry. Thus the transverse flow velocities of the one-dimensional theory become rotations in the experimental situation and centrifugal effects complicate the flow, mainly through a $\underline{J}_\theta \times \underline{B}_r$ force. However the main features of the theoretical flow pattern are produced experimentally.

Detailed measurements of the shock show a structure characterised by backward dispersion of damped magneto-acoustic waves.

ACKNOWLEDGEMENTS

The author is grateful to Dr J.W.M. Paul for many useful discussions and valuable suggestions, and to Dr R.J. Bickerton for his encouragement and support.

Thanks are due to Mr L.S. Holmes for his technical assistance.

REFERENCES

ANDERSON, J.E. 'MHD Shock Waves' M I T (1963).

BAZER, J. and ERICSON, W.B., Astrophys. J., 129, 758 (1958)

BICKERTON, R.J., LENAMON, L. and MURPHY, R.V.W., J. Plasma Phys., 5, 177 (1971).

BRATENAHL, A. and YEATES, C.M., Phys. Fluids, 13, 2696 (1970).

BURLAGA, L.F. and CHAO, J.K., J. Geophys. Res., 76, 7516 (1971).

CHAO, J.K. and OLBERT, S., J. Geophys. Res., 75, 6394 (1970).

CRAIG, A.D. and PAUL, J.W.M., Phys. Rev. Letts., 30, 681 (1973).

CRAIG, A.D. and PAUL, J.W.M., J. Plasma Phys., 9, 161 (1973).

KANTROWITZ, A. and PETSCHEK, H.E., 'Plasma Physics in Theory and Application', W.B. Kunkel, ed. (McGraw-Hill Book Company, Inc., N.Y., 1966).

PAUL, J.W.M., HOLMES, L.S., PARKINSON, M.J. and SHEFFIELD, J., Nature, 208, 133 (1965).

PETSCHEK, H.E., in AAS-NASA Symposium on the Physics of Solar Flares, ed. W. Hess (U.S. Gov. Printing Office, Washington D.C., 1964) NASA SP-50, p.425.

ROBSON, A.E. and SHEFFIELD, J. Third International Conference on Plasma Physics and Controlled Nuclear Fusion, Novosibirsk, (1968). Proceedings I A E A, Vienna, 1969, vol.1, p.119.

STRINGER, T.E., Plasma Physics (J. of Nuclear Energy Pt.C.) 5, 89 (1963).

(a)

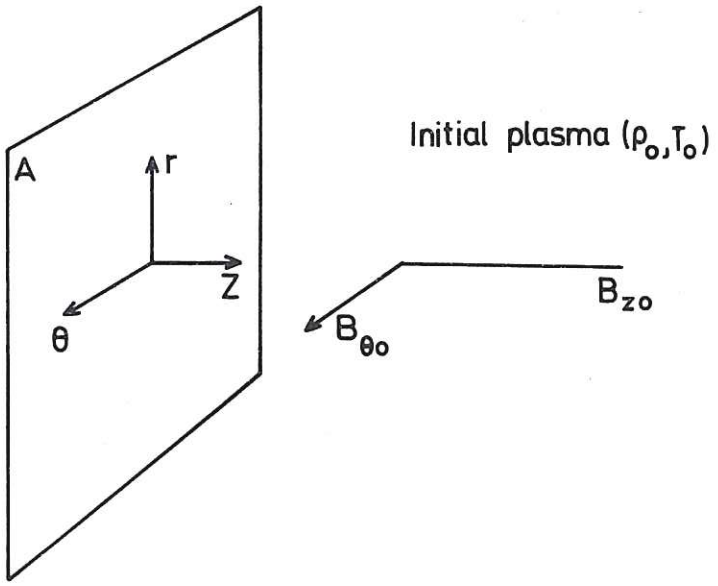

(b)

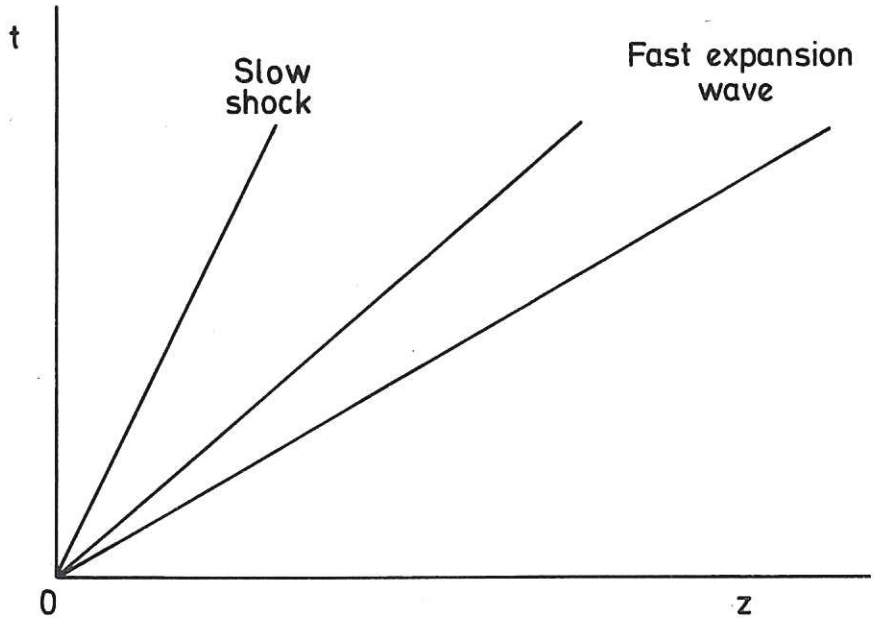

Fig.1 (a) Notation of launching process
(b) General flow pattern.

CLM-P 376

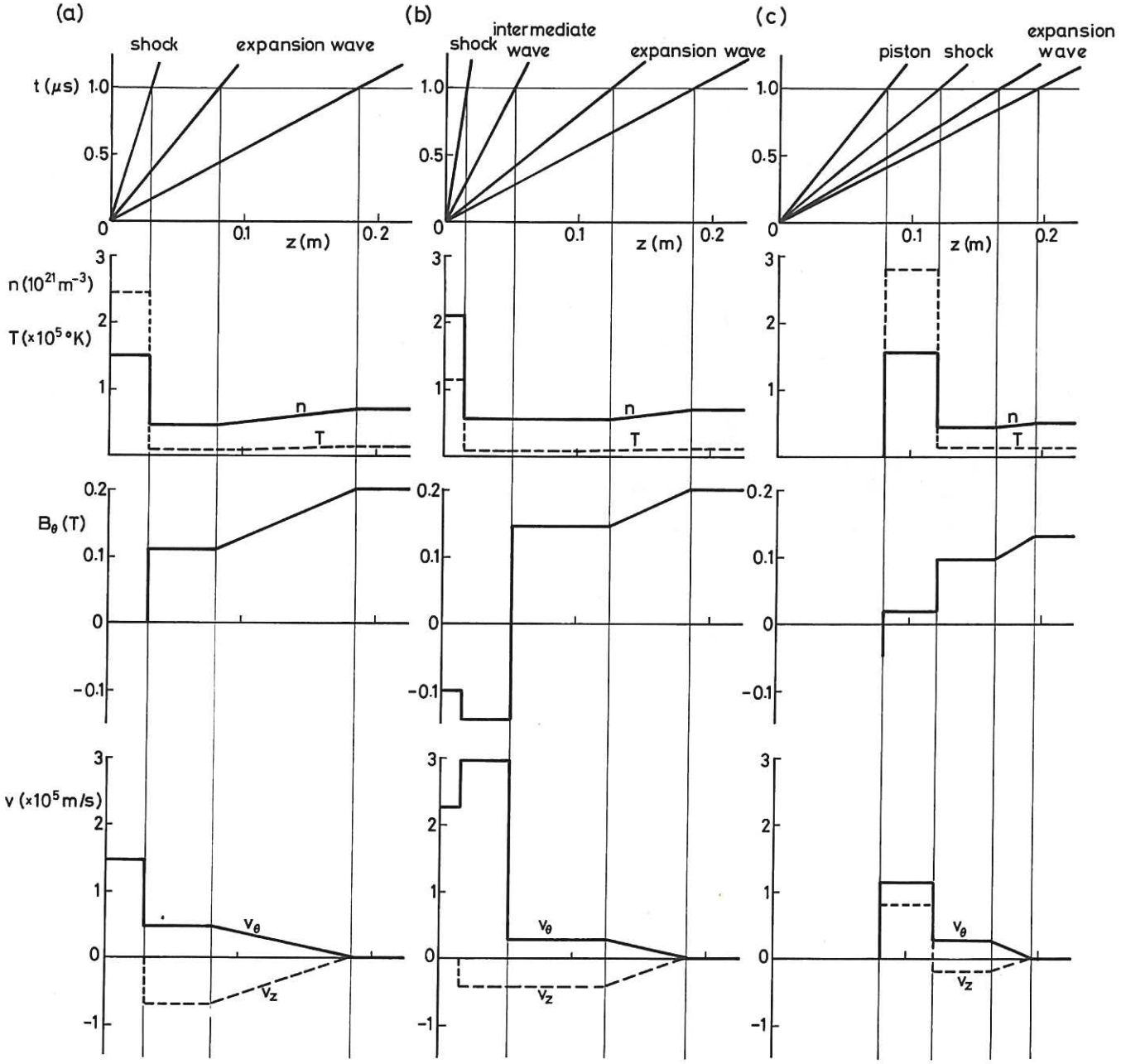

Fig.2 Theoretical Flow Patterns

(a) Ideal MHD model ($B_{\theta 2} = 0$)

(b) Ideal MHD model ($B_{\theta 2} < 0$)

(c) Finite piston velocity included.

CLM-P 376

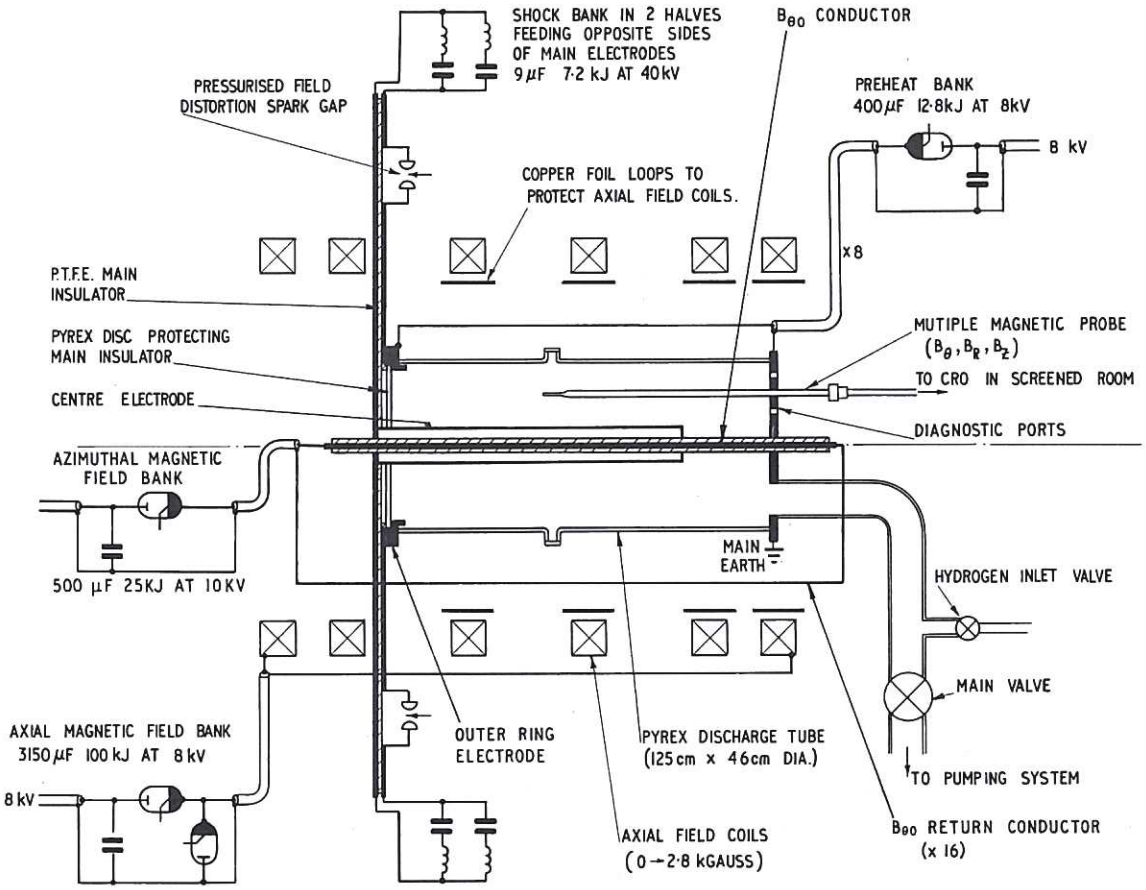

Fig.3 Schematic of the apparatus.

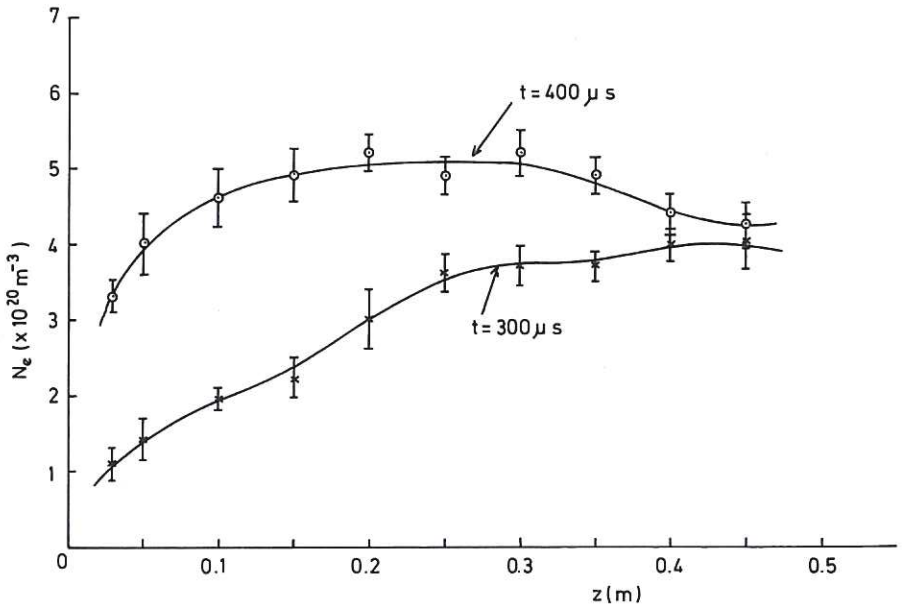

Fig.4 Axial distributions of n_e for the initial plasma (r = 142.5 mm, p = 20 mtorr, B_{zo} = 0.1 T, $B_{\theta o}$ = 0.13 T, standard deviations.

CLM-P 376

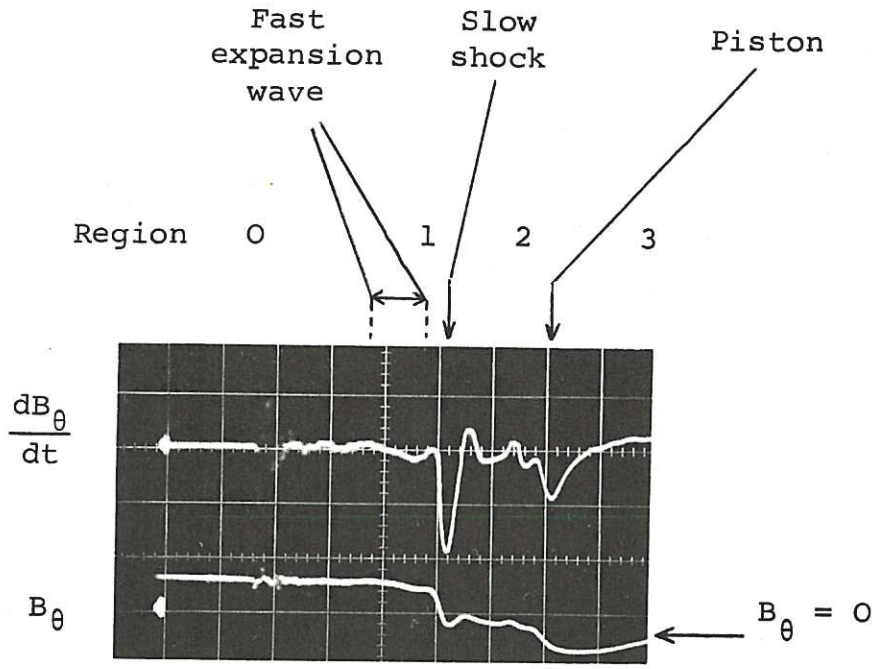

Fig.5 Typical B oscillogram (B_{zo} = 0.15 T, $B_{\theta o}$ = 0.13 T, r = 142.5 mm, z = 140 mm, p = 20 mtorr, time base = 0.5 μsec/div).

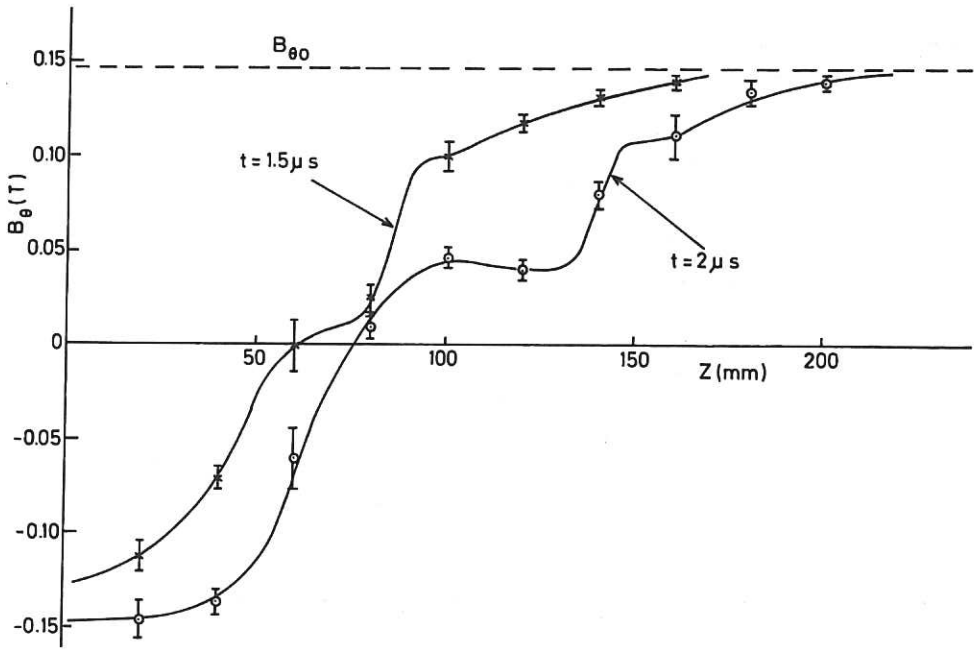

Fig.6 $B_\theta(z)$ distribution (B_{zo} = 0.15 T, $B_{\theta o}$ = 0.148 T, r = 125 mm, p = 20 mtorr, standard deviations).

CLM-P 376

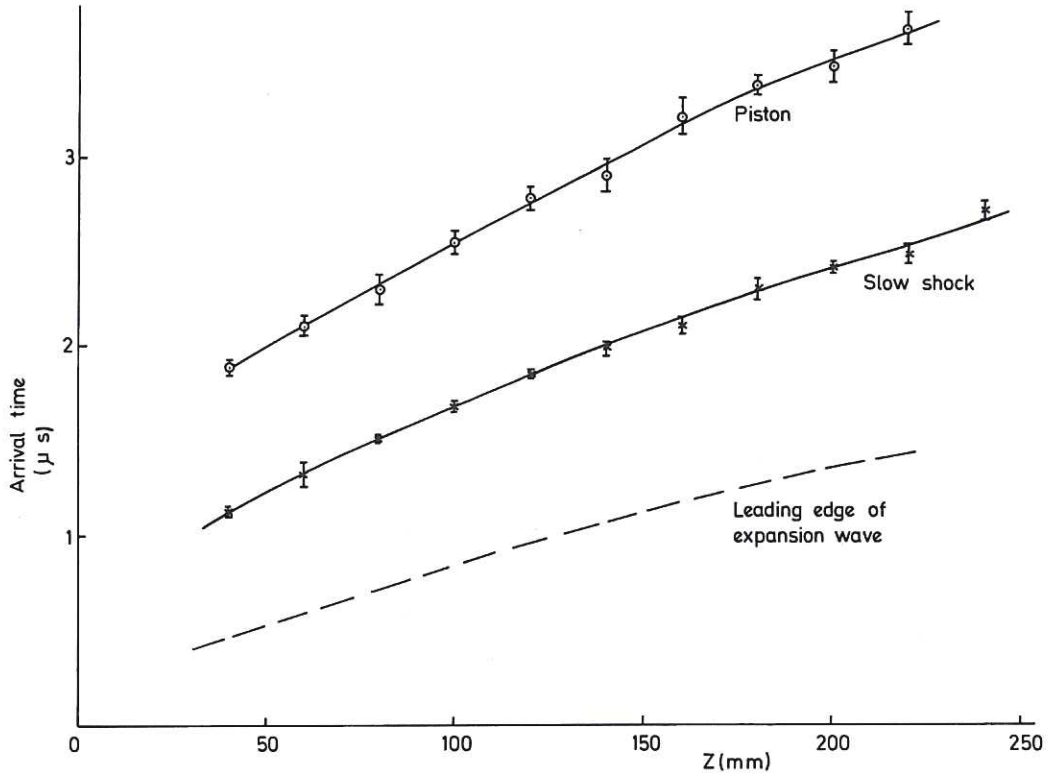

Fig.7 Axial propagation (B_{zo} = 0.15 T, $B_{\theta o}$ = 0.148 T, r = 125 mm, p = 20 mtorr, standard deviations).

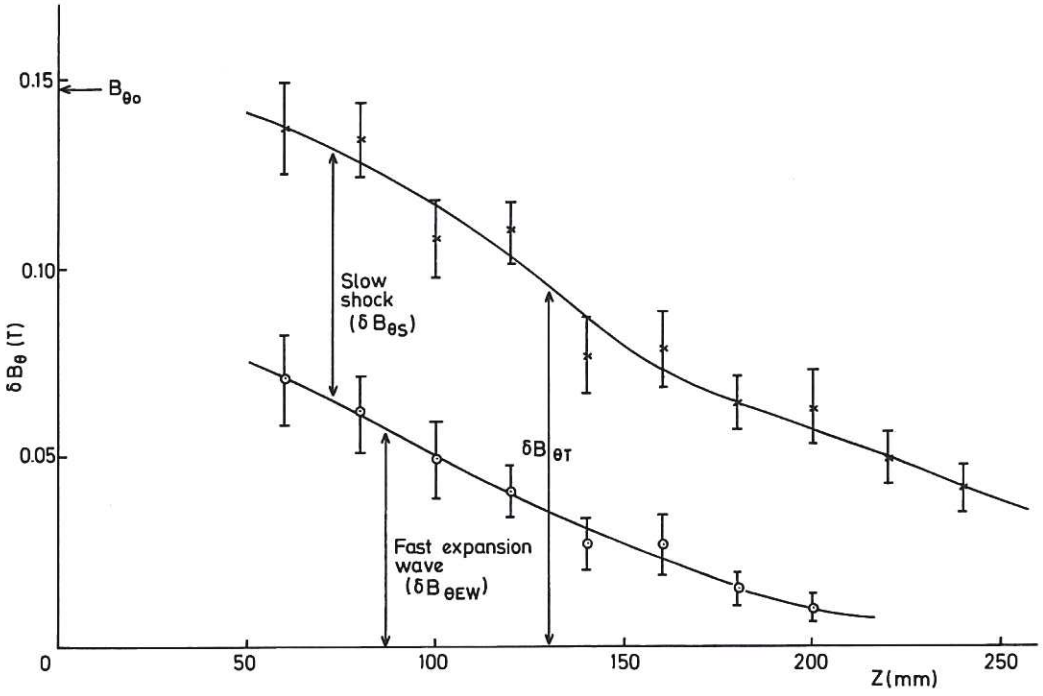

Fig.8 Axial variation of B_θ field changes occurring within the fast expansion wave and slow shock (B_{zo} = 0.15 T, $B_{\theta o}$ = 0.148 T, r = 125 mm, p = 20 mtorr, standard deviations).

CLM-P 376

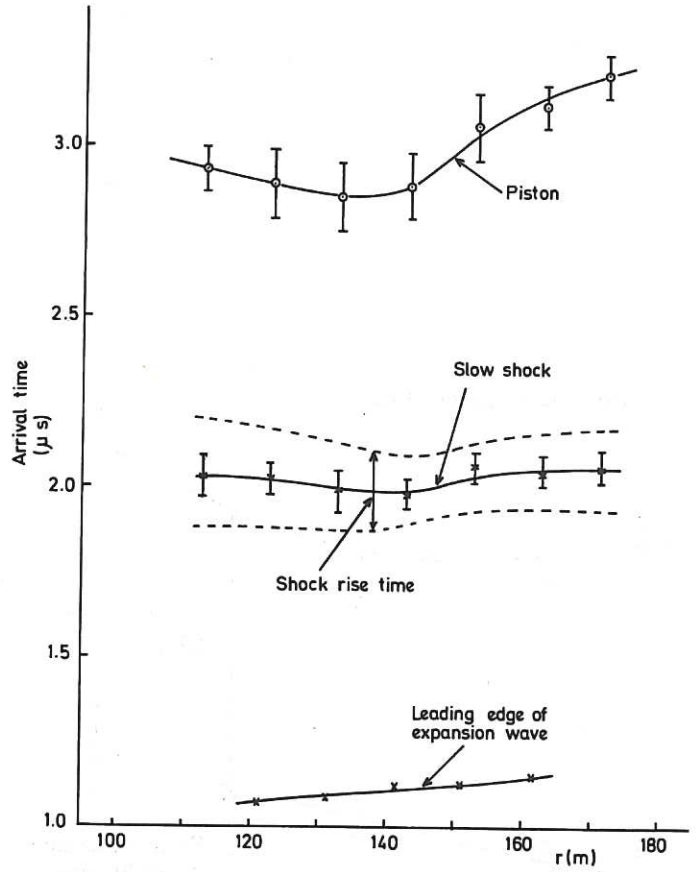

Fig.9 Radial variation in arrival time at z = 140 mm (B_{zo} = 0.15 T, $B_{\theta o}$ = 0.13 T at r = 142.5 mm, p = 20 mtorr, standard deviations).

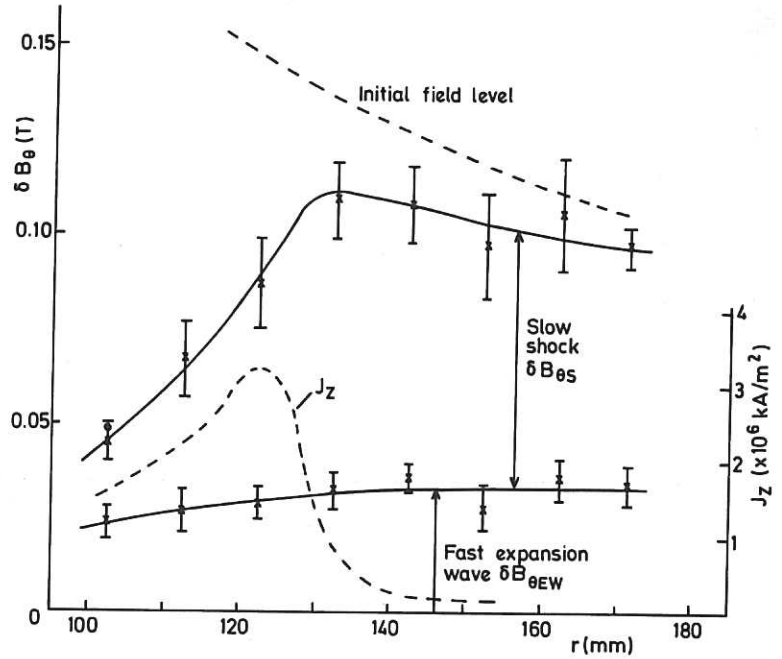

Fig.10 Radial variation of B_θ field changes occurring within the fast expansion wave and slow shock (B_{zo} = 0.15 T, z = 140 mm, p = 20 mtorr, standard deviations).

CLM-P 376

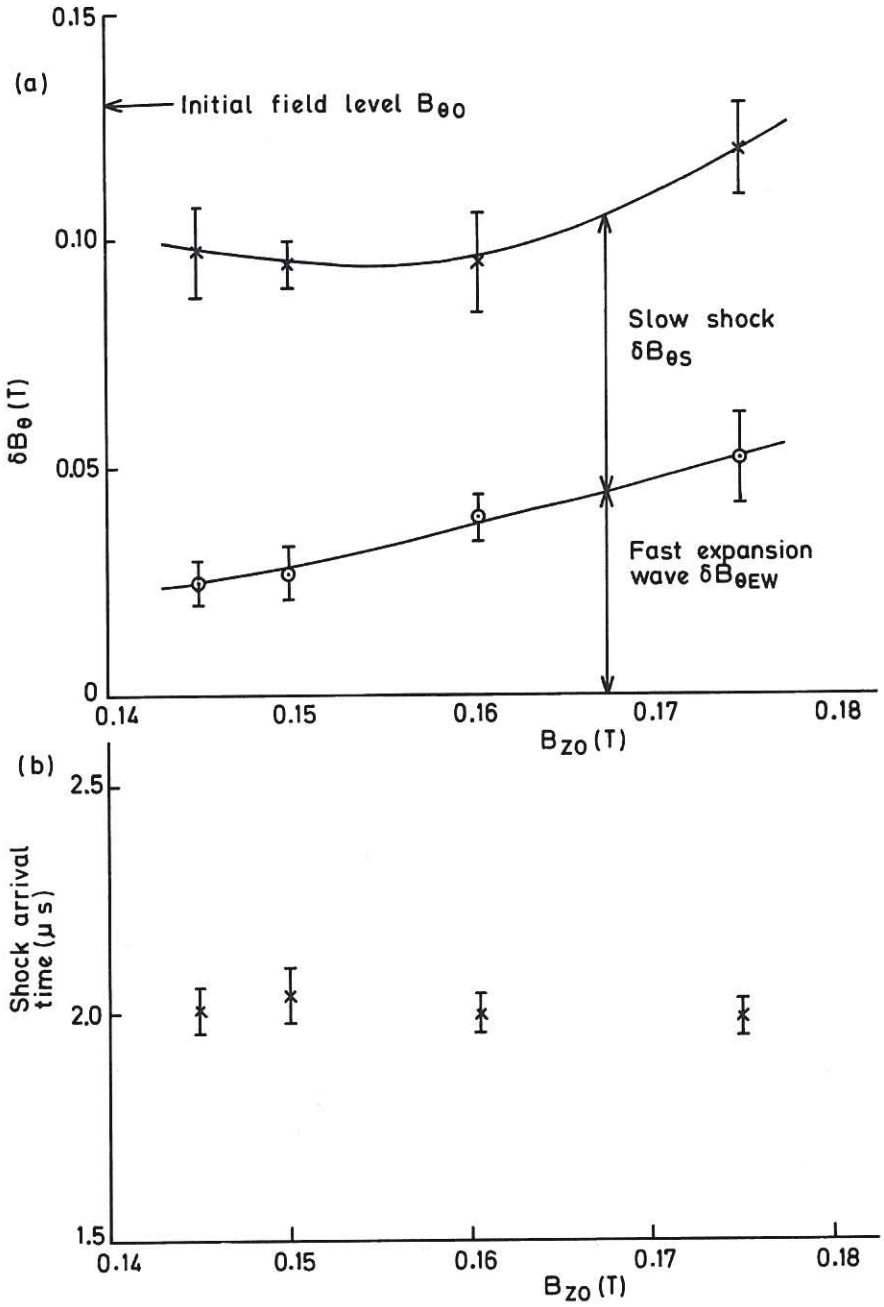

Fig.11 Variation with B_{zo} of (a) B_θ field changes occurring within the fast expansion wave and slow shock, (b) shock arrival time (z = 140 mm, r = 142.5 mm, $B_{\theta o}$ = 0.13 T, p = 20 mtorr, standard deviations).

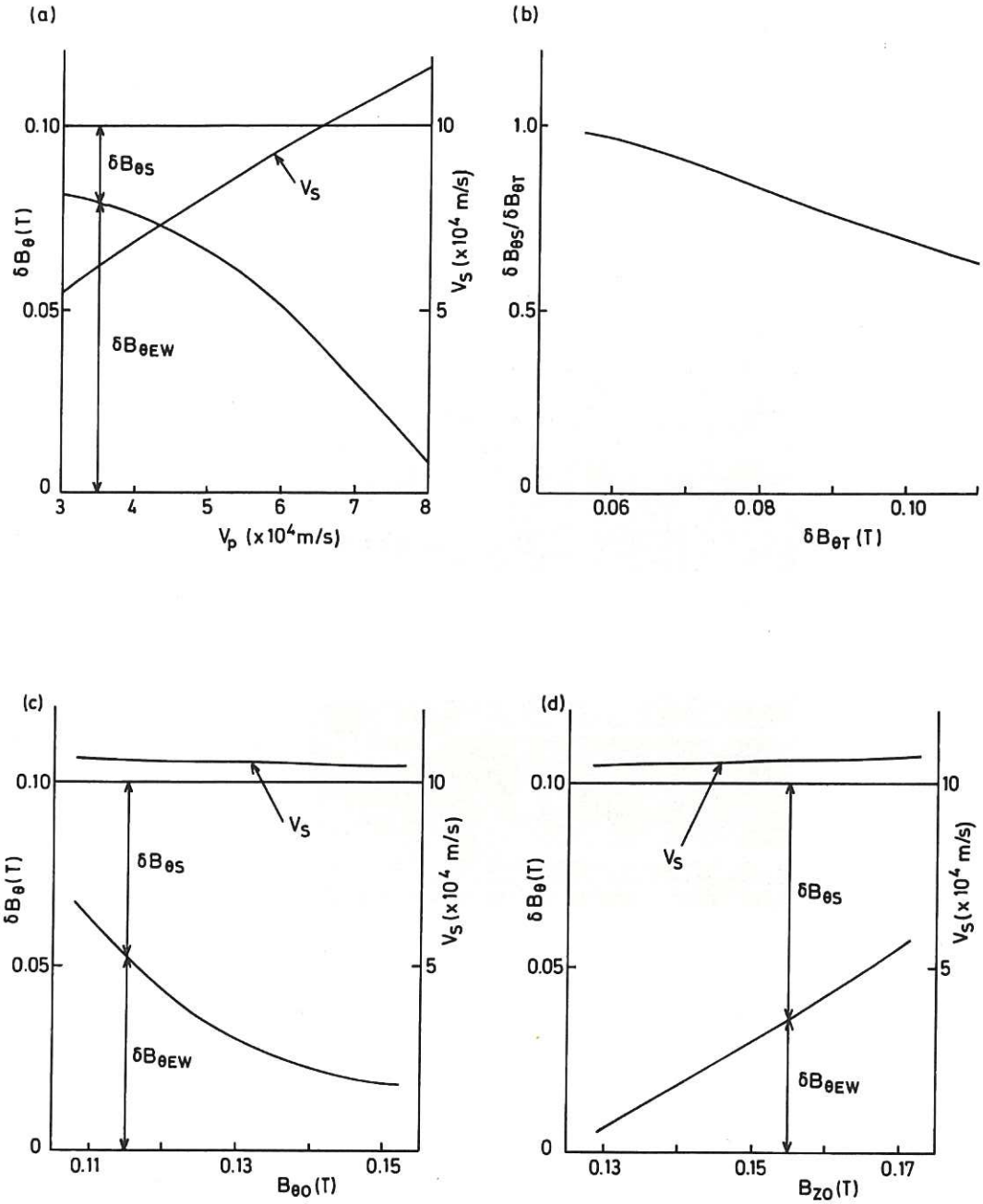

Fig.12(a) Theoreatical variation of $\delta B_{\theta EW}$, $\delta B_{\theta s}$ and V_s versus V_p (B_{zo} = 0.15 T, $B_{\theta o}$ = 0.13 T, $n_o = 6 \times 10^{20}$ m^{-3}, $T_o = 1.5 \times 10^4$ K).

(b) Theoretical variation of $\delta B_{\theta s}/\delta B_{\theta T}$ versus $\delta B_{\theta T}$ (B_{zo} = 0.15 T, $B_{\theta o}$ = 0.13 T, $n_o = 6 \times 10^{20}$ m^{-3}, $T_o = 1.5 \times 10^4$ K).

(c) Theoretical variation of $\delta B_{\theta EW}$, $\delta B_{\theta s}$ and V_s versus $B_{\theta o}$ (B_{zo} = 0.15 T, $n_o = 6 \times 10^{20}$ m^{-3}, $T_o = 1.5 \times 10^4$ K, $V_p = 7 \times 10^4$ m sec^{-1}).

(d) Theoretical variation of $\delta B_{\theta EW}$, $\delta B_{\theta s}$ and V_s versus B_{zo} ($B_{\theta o}$ = 0.13 T, $n_o = 6 \times 10^{20}$ m^{-3}, $T_o = 1.5 \times 10^4$ K, $V_p = 7 \times 10^4$ m sec^{-1}).

CLM-P 376

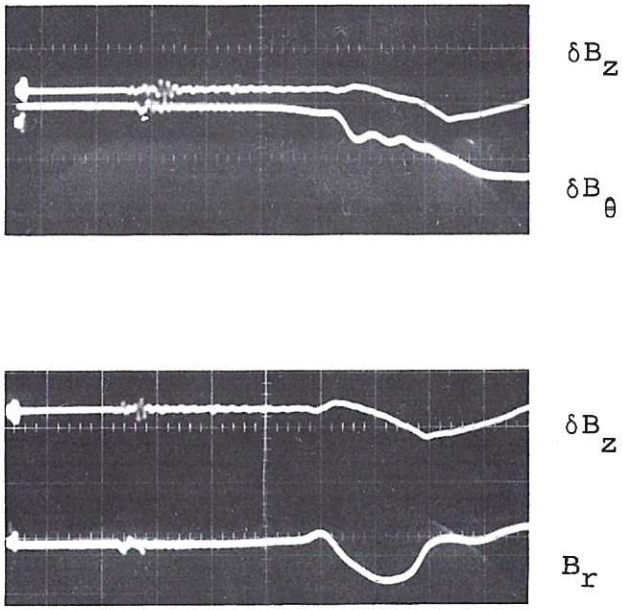

Fig.13 Typical oscillograms showing the relationship of the different field components (B_{zo} = 0.15 T, $B_{\theta o}$ = 0.13T, r = 142.5 mm, z = 140 mm, 0.14 T/div, 0.5 μsec/div).

CLM-P 376

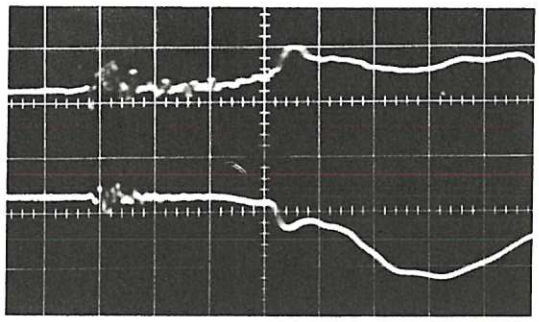

E_r (1.4 x 10^4 V/m / div)

B_θ (0.14 T/div)

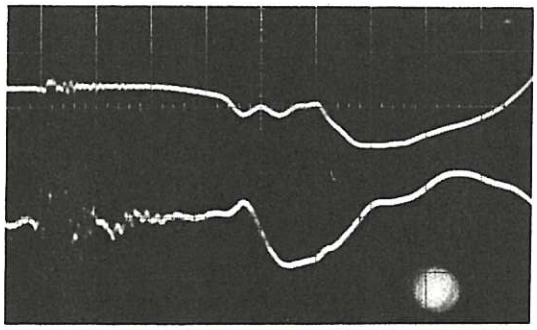

B_θ (0.14 T/div)

E_θ (1.4 x 10^4 V/m / div)

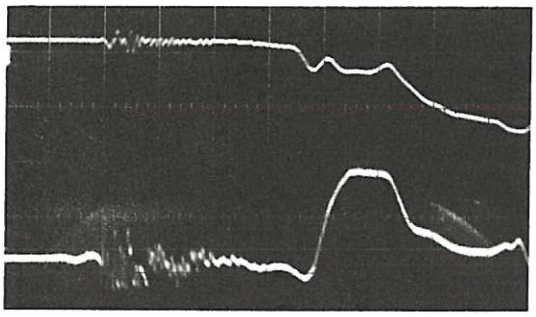

B_θ (0.14 T/div)

E_z (5 x 10^3 V/m / div)

Fig.14 Typical oscillograms of electric field components (B_{zo} = 0.15 T, $B_{\theta o}$ = 0.13 T, r = 142.5 mm, z = 140 mm, time base = 0.5 μsec/div).